Title

Catalytic visible light-driven alkane dehydrogenation by a di-uranyl germanotungstate

Journal

Chemical Science

ISSN

2041-6520

Authors

Tanuhadi, Elias

Herrera, Gabriel

Conour, Cambell S

et al.

Publication Date

2026-07-02

DOI

10.1039/d6sc01626j

ARTICLE

Received 00th January 20xx,
Accepted 00th January 20xx

DOI: 10.1039/x0xx00000x

Catalytic visible light-driven alkane dehydrogenation by a di-uranyl germanotungstate

Elias Tanuhadi[a,b,*], Gabriel Herrera[a,b], Cambell S. Conour[a,b] and Polly L. Arnold[a,b,*]

The dehydrogenation of alkanes to alkenes is an appealing strategy for upgrading abundant hydrocarbons, yet it is constrained by the inherent challenge of cleaving two inert C(sp^3)-H bonds with selectivity and without overoxidation. We report a cooperative photocatalytic dehydrogenation of unactivated cycloalkanes under visible light irradiation enabled by a new dinuclear uranyl complex supported by an oxidatively stable germanotungstate, $[NBu^n_4]_8[(UO_2)_2(GeW_{10}O_{34}(\mu_2\text{-}OH)_2)_2]\cdot(CH_3)_2CO$ (**1**). The uranyl complex catalytically converts cyclooctane to cyclooctene under ambient conditions with a TON per molecule of 44 and 9,10-dihydrophenanthrene to phenanthrene with a TON of 73 per molecule, using 1 mol% **1** in MeCN solution, under 427 nm irradiation, using $[S_2O_8]^{2-}$ or chloranil ($C_6Cl_4O_2$) as a sacrificial oxidant. The value of preorganization of two uranyl centers to yield the product of double hydrogen atom abstraction (HAA) is discussed in comparison with uranyl nitrate, $[UO_2(NO_3)_2(H_2O)_2]\cdot4H_2O$, the most widely studied uranyl photocatalyst, which is inactive for this reaction. A direct hydrogen atom transfer (d-HAT) mechanism with two HAA processes is proposed as trans-di-deuterated substrate (9S, 10S)-9,10-dihydrophenanthrene-9,10-d_2 ($C_{14}H_{10}D_2$) exclusively forms d_1 phenanthrene from abstraction of an H and a D atom from the same face.

Introduction

The importance of olefins as versatile and reactive building blocks for natural products and pharmaceutical agents has long been recognized. Consequently, their generation by a formal dehydrogenation of an inert alkane represents an attractive and potentially atom-economical target, sought equally by synthetic chemists and biological systems.[1]

Pioneering studies by Crabtree[2, 3] and Felkin[4] established catalytic transfer dehydrogenation of cyclooctane using tert-butylethylene (TBE) as a sacrificial hydrogen acceptor catalyzed by rare d-block complexes such as $(Me_2CO)(PPh_3)_2IrX$ (X = BF_4^- or SbF_6^-) (**Fig. 1a**). The d-block catalysts reported for this follow a C–H oxidative addition/β-hydride elimination mechanism. While the most active systems reach up to 58 turnovers (TO) min^{-1} for n-alkane/TBE transfer dehydrogenation at 200°C and can deliver up to 8752 TON after 10 h at 200 °C for n-octane/TBE transfer dehydrogenation at reduced catalyst loading (0.01 mol % Ir),[5] Goldman's $(C_6H_4P^{tBu2})_2P]IrCl$ system achieves maximum rates of 7.32 TO min^{-1} for n-octane/1-hexene transfer dehydrogenation at 100 °C (with 14.6 TO formed in the peak-activity window from 2–4 min).[6] Despite this progress, these platforms still rely on precious-metal catalysts and require elevated temperatures. Visible-light induced Hydrogen Atom Abstraction (HAA) routes to eliminate two H atoms from neighboring C–H groups offer an alternative, low-energy mechanism for dehydrogenation. To this end, the decatungstate ion, most commonly used as its tetra-n-butylammonium salt ($[TBA]_4[W_{10}O_{32}]$, TBADT; TBA = $N(Bu^n)_4$), has demonstrated excellent activity as a photocatalyst for a single HAA from various organic substrates.[7] TBADT is part of the large family of polyoxometalates (POMs),[8] structurally versatile, anionic metal-oxide clusters with tunable redox and electronic properties that have found applications across catalysis,[9, 10] electrochemistry,[11] magnetochemistry,[12] and biology.[13, 14] Owing to the strong W=O bond (BDE = 700–800 kJ mol^{-1}),[15] TBADT displays HAA reactivity different from that of typical transition metal oxo complexes because in the latter, the carbon radical formed from the HAA tends to react further in a 'rebound process' resulting in alkane hydroxylation rather than dehydrogenation.[16-18] Photocatalytic dehydrogenation using TBADT has been demonstrated under UV-light irradiation (λ = 323 nm).[19] One cleverly designed multicomponent system added a cobaloxime co-catalyst, which enabled the formation of cyclooctene in 19 % yield, presumably *via* the formation of a cobalt hydride; release of H_2 and the 88 kcal mol^{-1} of energy per photon provided by UV irradiation makes this endergonic.[20] This multicomponent approach has been successful for other

[a] *Dept of Chemistry, University of California, Berkeley, Berkeley, CA, 94720, USA. E-mail: pla@berkeley.edu, elias.tanuhadi@berkeley.edu*
[b] *Chemical Sciences Division, Lawrence Berkeley National Laboratory, Berkeley, CA 94720, USA.*

Electronic Supplementary Information available: synthetic and mechanistic details.

endergonic reactions such as aromatization. These important advances rely on spatially separated elementary steps distributed across multiple catalyst components that must be carefully orchestrated for rates and reagent compatibility. [21, 22] Moreover, C–H bond selectivity has not yet been demonstrated for TBADT beyond reliance on the intrinsic electronic properties.

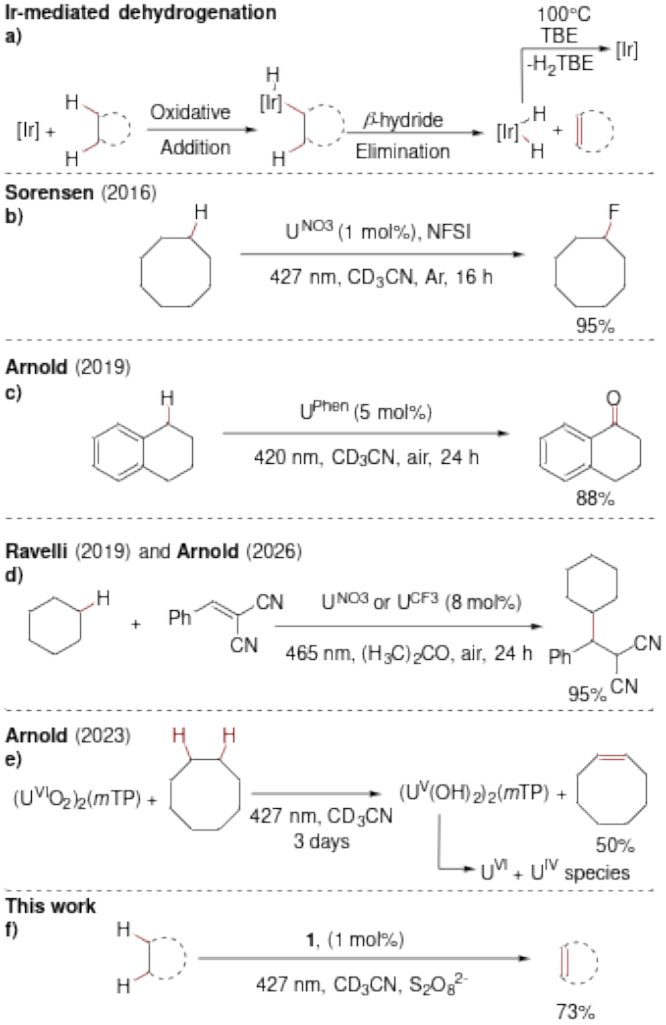

Figure 1 (a) Thermally driven molecular Ir-catalyzed transfer dehydrogenation using tert-butyl ethylene (TBE) as a sacrificial alkene for turnover. Panels b–e: overview of uranyl(VI) photocatalysts for visible-light C(sp^3)–H hydrogen atom abstraction (HAA). Previous examples include **(b)** the uranyl nitrate ($[UO_2(NO_3)_2(H_2O)_2]\cdot 4H_2O$) mediated C-H fluorination (Sorensen, 2016, top), **(c)** benzylic C–H oxidation (Arnold, 2019), and **(d)** C–H to C–C bond formation via radical addition to an electrophilic olefin (Ravelli, 2019, Arnold 2026). **(e)** While substoichiometric visible-light-driven dehydrogenation of cyclooctane to cyclooctene in the presence of $(U^{VI}O_2)_2$(mTP) is made possible by the di-nuclear nature of the system, the process is rendered non-catalytic by the oxidative decomposition of the complex. **(f)** This work introduces a POM-scaffolded di-uranyl complex, enabling visible light driven photocatalytic hydrocarbon dehydrogenation.

The visible-light-induced HAA by the U(VI) uranyl ion ($[UO_2]^{2+}$), the predominant, earth-abundant form of uranium in the environment, represents a mild and potentially energy-efficient route to hydrocarbon functionalization.[23] Upon excitation with ~420 nm light, uranyl complexes undergo a ligand-to-metal charge transfer (LMCT) to access a highly reactive excited state that can functionalize organic substrates via direct hydrogen atom transfer (d-HAT) or single-electron transfer (SET).[24]

Uranyl nitrate, $[UO_2(NO_3)_2(H_2O)_2]\cdot 4H_2O$, **$U^{NO3}$**, is the most widely studied uranyl photocatalyst. Early work by Bakac demonstrated UV-driven aerobic oxidation of aqueous organics.[25, 26] Recent studies recognized that visible-light excited uranyl complexes can be used in organic solvents to catalyze alkane C–H bond functionalization. In 2015, Sorensen and co-workers reported that **U^{NO3}** enables efficient alkane C–H fluorination (e.g., cyclooctane to fluorocyclooctane in >95% yield with a 1 mol% catalyst) (**Fig. 1b**).[27] In 2019, we reported the uranyl–phenanthroline complex $[UO_2(NO_3)_2(Ph_2phen)]$ (Ph_2phen = 4,7-diphenyl-1,10-phenanthroline), **U^{Phen}**, as a selective photocatalyst for C–H oxidation of a range of substrates including benzylic molecules that **U^{NO3}** is normally inactive towards, and C–C bond cleavage in a lignin model (**Fig. 1c**).[28, 29] Recently, we showed that the coordination of benzoate ancillary ligands in the equatorial plane leads to particularly reactive catalysts with steered reactivity toward more sterically accessible C–H bonds by modulation of the steric environment around the uranyl-oxo group (**Fig. 1d**).[30, 31]

Studies on these systems support a general mechanism in which the excited uranyl unit initiates reactivity through HAT to generate carbon-centered radicals allowing for C–E bond formation (E = F, C, N).[28, 29] We hypothesized that two adjacent uranyl cations could provide a base-metal derived catalytic system capable of HAA-led dehydrogenation, since the strong U–O bond prevents the unwanted oxidation of a substrate that is observed in catalytic oxidations by thermally activated d-block metal oxo catalysts and reported the stoichiometric dehydrogenation of cyclooctane (50% yield) using the visible – light activated di-uranyl complex $\{(UO_2)(py)_2\}_2(mTP)_2$, where mTP is a tetraphenolate that supports two neighboring uranyl dications $\{2\text{-}(OC_6H_2\text{-}2\text{-}^tBu,4\text{-}Me)_2CH\}\text{-}1,3\text{-}C_6H_4$ (**Fig. 1e**). Unfortunately, turnover was hampered by the oxidative decomposition of the ligated complex.[32] Thus, we turned to an oxidatively stable alternative to organic ligands, lacunary POMs,[33] a subclass of POMs that are derived by extrusion of framework metal cations via controlled basic hydrolysis, to generate rigid, multidentate, all-inorganic ligands that should provide an oxidation-resistant supporting framework for these photocatalysts. Uranyl-containing POMs have previously been explored as catalysts for other transformations including cyclization, condensation, and oxidative coupling reactions.[34-36] While these are usually made in protic media as alkali-metal salts, for this work we prepared alkylammonium–uranyl–POM complexes which are compatible with hydrocarbon substrates and fully anaerobic environments, enabling us to avoid complications arising from water- and proton-dependent

hydrolysis, ion exchange, aggregation, or rearrangement of the POMs.[37-40]

Here, we report the first fully characterized example of cooperative photocatalytic dehydrogenation of unactivated cycloalkanes enabled by the new polyoxometalate-stabilized di-uranyl scaffold $[NBu^n_4]_8[(UO_2)_2(GeW_{10}O_{34}(\mu_2\text{-}OH)_2)_2]\cdot(CH_3)_2CO$ (**1**). Under optimized conditions, yields of up to 73% (TON per molecule = 73) can be achieved (**Fig. 1f**). Supported by a set of photoluminescence, labelling, and kinetic studies, we demonstrate how this system harnesses the structural preorganization and oxidative stability of POMs to position two $\{U^{VI}O_2\}^{2+}$ centers in close proximity, unlocking cooperative reactivity inaccessible to mononuclear uranyl complexes and establishing a new design principle for actinide photocatalysis.

Results and discussion

Synthesis and structure

The synthesis of **1** starts with the preparation of the literature-reported lacunary precursor $[NBu^n]_4[\gamma\text{-}Ge^{IV}W_{10}O_{34}(H_2O)_2]$ (H_2**GeW$_{10}$**).[37] Upon addition of solid $(UO_2)(acac)_2$ (acac = acetylacetonate) to a clear, colorless solution of one equiv of H_2**GeW$_{10}$** in acetone/water (1.6% v/v) (**Scheme 1, S1**) at 25°C, an immediate color change to yellow is observed. After 90 min, filtration of the reaction mixture at RT afforded a yellow solution from which yellow block-shaped crystals of the target molecule $[NBu^n_4]_8[(UO_2)_2(GeW_{10}O_{34}(\mu_2\text{-}OH)_2)_2]\cdot(CH_3)_2CO$ (**1**) were obtained in a yield of 25% based on U from a mixture of acetone and diethyl ether (~5:1, (v/v)) within approximately 24 h. This is pleasing considering the low stability of [γ-XW_{10}] units (X = Si^{IV}, Ge^{IV}, P^V), as higher reaction temperatures could have resulted in undesired isomerization and/or partial decomposition of the lacunary units.[40, 41]

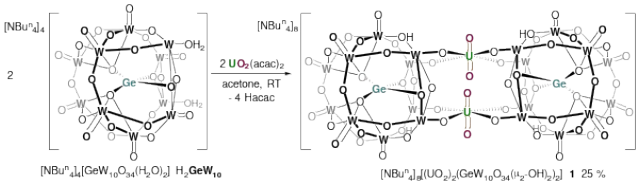

Scheme 1 Synthesis of $[NBu^n_4]_8[(UO_2)_2(GeW_{10}O_{34}(\mu_2\text{-}OH)_2)_2]$ (**1**) from lacunary $[NBu^n_4]_4[GeW_{10}O_{34}(H_2O)_2]$ and uranyl acetylacetonate in acetone.

A single-crystal X-ray diffraction (SXRD) study of **1** reveals that the polyanion of **1** crystallizes in the orthorhombic space group Pbca with idealized C_{2v} point group symmetry (**Table S1**). The polyanion of **1** is composed of two [γ-$GeW_{10}O_{35}$] lacunary units linked by two $\{UO_2\}^{2+}$ ions that bind through four equatorial binding sites on each polyoxotungstate. Each U^{VI} center adopts a distorted octahedral coordination environment, featuring two U=O oxo bonds with lengths ranging from 1.697(1) to 1.742(3) Å. The separation between the two U^{VI} centers is 5.5097(14) Å, while the distance between the endo uranyl -oxo ligands, O_{endo}–O_{endo} is 2.6157(14) Å (**Fig. 2**).

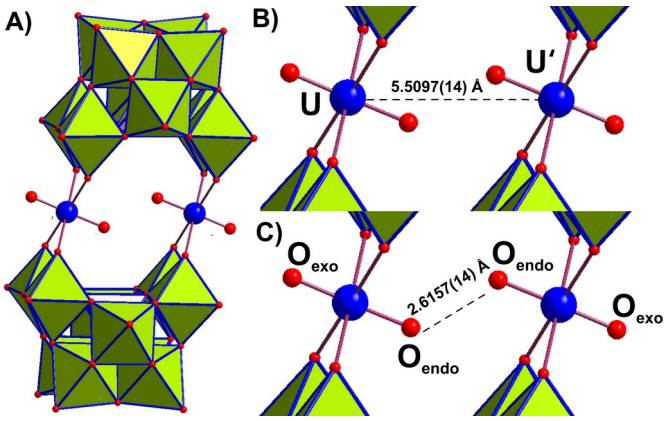

Figure 2 Crystal structure of **1** showing **(a)** the polyhedral frontal view of the anion and **(b)** the distance between the two pseudo-octahedrally coordinated $[UO_2]^{2+}$ centers and **(c)** between two terminal oxo ligands. U^{VI} and O atoms are shown as blue and red spheres, respectively; Ge^{IV} are shown as grey tetrahedra and $\{WO_6\}$ units are shown as green polyhedra. Tetra-n-butyl ammonium counter cations, H, and lattice solvent molecules are omitted for clarity.

Besides SCXRD, **1** was characterized by ATR-IR spectroscopy (**Fig. S1**) showing the terminal W=O and bridging W–O–W vibrations typical for a Keggin-type polyoxotungstate framework.[37, 42] The bands at 1632, 1702, 2872 and 2958 cm^{-1} are attributed to vibration and deformation bands of TBA methylene groups. A band at 950 cm^{-1} can be assigned to the asymmetric O=U=O stretching vibration, $\nu_{as}(UO_2)$, and falls within the range reported for uranyl-containing heteropolyoxometalates, including $[H_3O]_4[Ni(H_2O)_3]_4\{Ni[(UO_2)(PO_3C_6H_4CO_2)]_3(PO_4H)_4\cdot 2.72H_2O$, for which antisymmetric UO_2 stretching modes at 932.8 and 969.7 cm^{-1} have been reported. This value is also comparable to that of related uranyl sandwich-type POMs such as $[(UO_2)_2(H_2O)_2(SbW_9O_{33})_2]^{14-}$ and $[(UO_2)_2(H_2O)_2(TeW_9O_{33})_2]^{12-}$, where uranyl units are similarly bound in oxo-donor polyoxotungstate environments (Fig. S1 and S38).[43] The 950 cm^{-1} band is also close to those in the relatively electron-poor uranyl nitrate and chloride benchmarks, including $UO_2(NO_3)_2(H_2O)_6$ (949 cm^{-1}),[44] $[UO_2(NO_3)_3]^-$ salts (959(2) cm^{-1}),[45] and $[UO_2Cl_2(MeCN)_3]$ (953 cm^{-1}),[29] but at higher energy than the Ph_2phen-ligated uranyl chloride catalysts (922 and 900 cm^{-1}) that we previously reported.[29] Thus, **GeW$_{10}$** provides a comparatively electron-poor oxo-donor environment while pre-organizing two adjacent photoactive uranyl sites.

The exact composition including the lattice solvent molecules in crystalline **1** was determined using thermogravimetric analysis (TGA) (**Fig. S2**). Two weight-loss regions (**Table S2**) that are attributed to losses of acetone from the lattice and TBA cations, respectively, can be observed (**Fig. S2**). The ^{1}H NMR spectrum of a CD_3CN solution of **1** contains CH_2 and CH_3 resonances that can be assigned to the TBA cations and acetone (**Fig. S3**).

Photophysics of 1

Table 1 Photocatalytic dehydrogenation of hydrocarbons.[a]

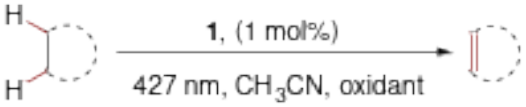

Entry	Catalyst	Deviation from standard conditions	Major (minor) product(s)	Yield [%][b]
1	**1**	—	Cyclooctene	16
2	**1**	No H_2O	Cyclooctene	26
3	**1**	67h irradiation, no H_2O	Cyclooctene	44
4	**1**	Chloranil ($C_6Cl_4O_2$) as oxidant	Cyclooctene	19
5	**1**	Cycloheptane instead of cyclooctane	Cycloheptene	1.6
6	**1**	9,10 DHP instead of cyclooctane	Phenanthrene	73
7	**1**	No light	—	0
8	—	—	—	0
9	**GeW_{10}**	—	—	0
10	**1**	In acetone	—	0
11	**U^{NO3}**	—	—	0
12	**U^{SO4}**	—	—	0
13	**U^{CF3}**	—	—	0
14	**1**	$TBA_2S_2O_8$ as an oxidant	But-1-ene (cyclooctene)	19.4 (9.7)
15	**1**	$TBA_2S_2O_8$ as an oxidant, NMR-scale reaction, no stirring	But-1-ene (cyclooctene)	24.2 (4.8)
16	**1**	No oxidant	—	0

[a]standard conditions, 1 equiv. $Na_2S_2O_8$ and 1 equiv. hydrocarbon, RT, H_2O/acetonitrile (1:6.25), irradiation with a 52 W Kessil PR160L 427 nm lamp for 24 h, 1000 rpm. [b] The yield of the dehydrogenated product was calculated by comparing the integral of the multiplet assigned to the olefinic C-H (2H) to the methyl acetate peak (3.67 – 3.45 ppm, m, 3H).

The UV/vis spectrum of **1** is characterized by an absorption maximum at 270 nm (ε = 69 928.1 $M^{-1}cm^{-1}$) attributed to the $p\pi(O_{bridging}) \rightarrow d\pi^*(W)$ ligand-to-metal charge-transfer typical for the Keggin-type framework (**Fig. S5** and **S6**).[46] A second absorption at 427 nm (ε = 126.3 $M^{-1}cm^{-1}$) with vibronic coupling, characteristic of the uranyl ion absorption, is observed.[47] Photoluminescence studies of a CH_3CN solution of **1** display an excitation spectrum with peaks at 357 nm and 429 nm and an emission spectrum (λ_{Exc} = 427 nm) consisting of two bands which are observed at 504 nm and 524 nm, respectively (**Fig. S7**).[29] Considering the irreversibility of the $U^{VI/V}$ redox couple ($E_{p,c}$ = −1.03 V vs Fc/Fc^+ in CH_3CN), the Rehm−Weller formalism could not be applied to predict the excited state redox potential $E_{1/2}$* of **1** (**Fig. S4**).

Photocatalysis

To probe the photocatalytic dehydrogenation activity of **1**, a H_2O/CH_3CN (1:6.25) solution of 0.6 mM **1**, 60 mM cycloalkane substrate and 60 mM oxidant ($S_2O_8^{2-}$ or chloranil, $C_6Cl_4O_2$) to turn over the catalyst[48] was prepared under an N_2 atmosphere and irradiated at 427 nm for 24 h at 25 °C. IR spectroscopy confirms that **1** retains its characteristic structural features under these catalytically relevant solution conditions, with the diagnostic uranyl asymmetric stretch and POM framework vibrations matching those observed in the solid-state spectrum (**Fig. S38**).

The yields of the dehydrogenated products were calculated by integration of NMR spectra of aliquots against an internal standard (**Fig. S14** and **S15**) and are summarized in **Table 1**. No oxygenated products were observed in the ^1H NMR spectra throughout catalysis. Dehydrogenation of cyclooctane (COA) to yield cyclooctene (COE) is observed in 16% yield (NMR yield is based on relative integration against CH_3COOCH_3 as an external standard) for **1** after 24h (entry 1 **Table 1** and **Fig. S16**). A hydroxylation–dehydration pathway[49] is unlikely because the reaction also proceeds under rigorously anhydrous conditions with yields in COE of up to 26% after 24 h, corresponding to 26 TON per molecule (entry 2 **Table 1** and **Fig. S17**), reaching 44% COE after 67h (entry 3 **Table 1** and **Fig. S18**). Quantitative ^1H NMR spectroscopic studies show that the TBA counter cations remain unchanged over the course of the catalysis (**Fig. S19** and **S20**). Catalytic turnover can be achieved using different oxidants other than $S_2O_8^{2-}$, (e.g. chloranil, $C_6Cl_4O_2$, entry 4 **Table 1** and **Fig. S21**). Reactions performed with $TBA_2S_2O_8$ produced but-1-ene, consistent with the degradation of the TBA cation via a Hofmann-type mechanism (**Scheme S3** and **Fig. S41** and **S42**). This byproduct was detected under homogeneous bulk reaction conditions and in slightly greater quantities under NMR-scale conditions (entries 14 and 15 **Table 1**). We attribute this difference to the use of $TBA_2S_2O_8$ as a soluble oxidant and, in the NMR-scale experiment, to inefficient mixing in the sealed J. Young NMR tube. The catalytic dehydrogenation does not proceed in the absence of an oxidant (**Fig. S25** and entry 16 Table 1).

The dehydrogenation of cycloheptane (CHA) gives cycloheptene (CHE) in only 1.6% yield (entry 5 **Table 1** and **Fig. S22**); no dehydrogenation products are detected for cyclohexane or cyclopentane (**Figs. S23 – S25**), in line with Stern−Volmer quenching experiments for mixtures of **1** with cycloalkanes of varying ring size, which show progressively weaker quenching with decreasing ring size supporting a direct H-atom-transfer pathway (**Figs. S8–S13**).[49] The dehydrogenation of 9,10-dihydrophenanthrene (DHP) to phenanthrene proceeds with 73% yield (TON = 73) (entry 6 **Table 1** and **Fig. S26**).

The reaction does not proceed in the absence of light or catalyst (entry 7 **Table 1**; entry 8 **Table 1** and **Fig. S28** and **S29**). Reaction mixtures containing **GeW_{10}** (entry 9, **Table 1** and **Fig. S30**) do not give any dehydrogenated products. The use of acetone as reaction solvent yields no observed cyclooctene formation but we attribute this to the low solubility of **1** (entry 10 **Table 1** and **Fig. S31**).

Mechanistic aspects of the desaturation

We were keen to understand the importance of the pairing of the adjacent photoexcitable uranyl ions in effecting the abstraction of two adjacent *cis* hydrogen atoms. First, we studied the capacity of the best mononuclear uranyl HAA catalysts.[50] **U^{NO3}** (entry 11 **Table 1** and **Fig. S32**) and **U^{SO4}** (entry 12 **Table 1** and **Fig. S33**) result in traces of dehydrogenated product. Mononuclear uranyl tris–benzoate complex K(THF)$[\{(F_3C)_2C_6H_3CO_2\}_3UO_2]$, **$U^{CF3}$**, which we showed is particularly inert towards the disproportionation of U^V into U^{VI} and insoluble

U^{IV}, results in formation of a grey precipitate and only traces of COE (entry 12 **Table 1** and **Fig. S34, S35**). To our knowledge, TBADT has not demonstrated double HAT on C–H bonds.[20]

Photolysis of a 2:2:1 mixture of cyclooctane, $S_2O_8^{2-}$ and TEMPO in the presence of 1 mol % **1** results in the formation of 1-(cyclooctyloxy)-2,2,6,6-tetramethylpiperidine (**2**) (**Scheme S2** and **Fig. S39**). This is the addition product of the cyclooctyl radical to TEMPO. In a complementary spin-trapping experiment, dehydrogenation of cyclooctane in the presence of 1.5 equiv. DMPO (**Scheme S3**) gave an EPR signal assigned to the corresponding COA-DMPO nitroxide radical adduct (**Fig. S40**). Together, these experiments support a radical pathway for the dehydrogenation.

In contrast to persulfate-initiated methane functionalization in strongly acidic sulfate media,[51] where $CH_3^{\cdot}$ can be intercepted to give methyl bisulfate and related sulfate esters, we do not detect any organo-sulfate products in our reactions turned over with $S_2O_8^{2-}$. We also tested bibenzyl ($Ph(CH_2)_2Ph$) as a qualitative probe under these conditions, since a benzylic radical intermediate would be expected to be particularly susceptible to sulfate trapping.[49] Again, no sulfonated or sulfate-ester products are observed by GC-MS (**Fig. S36** and **S37**). This argues against a freely diffusing carbon-radical pool and for the role of $S_2O_8^{2-}$ as an outer-sphere oxidant.

Kinetic studies on a photolyzed 1:1 mixture of C_8H_{16} or C_8D_{16} and $TBA_2S_2O_8$ in in the presence of 1 mol% **1** in CD_3CN (**Scheme S4** and **Fig. S41 – S50**) reveal a primary kinetic isotope effect of k_H/k_D = 3.17 (**Fig. S46** and **S47**), suggesting that the first C–H bond cleavage by **1** is the rate determining step of the overall reaction. The initial rate of the reaction does not change with different concentrations of $TBA_2S_2O_8$ (**Fig. S48 – S50**) demonstrating that the turnover of the uranyl catalysts by $S_2O_8^{2-}$ is not involved in the overall rate law.

We also considered whether oxo sites of the GeW_{10} framework could participate in the second HAA step. Direct thermal HAA at a ground-state tungsten-oxo site is unlikely on thermodynamic grounds since reported BDFE(O–H) values for reduced and protonated tungsten-oxo sites in Keggin-type polyoxotungstates such as $[PVW_{11}O_{40}]^{5-}$ or $[PW_{12}O_{40}]^{4-}$, are only *ca.* 43–48 kcal mol^{-1}.[52, 53] These values are substantially lower than the C–H bond strengths of cyclooctane (95–97 kcal mol^{-1}), and even the benzylic C–H bonds in 9,10-dihydrophenanthrene (76–80 kcal mol^{-1}). To experimentally assess whether a polyoxotungstate could mediate the second HAA step following initial uranyl-driven HAA, a control reaction combining uranyl with TBADT, $[TBA]_4[W_{10}O_{32}]$, was performed under otherwise comparable 427 nm irradiation conditions. No detectable dehydrogenation product was observed (**Fig. S51**).

Although these data argue against direct HAA by a ground-state tungsten-oxo site, they do not uniquely define the identity of the second H-transfer site under catalytic conditions. We therefore assign the second HAA step cautiously to the preorganized di-uranyl/POM pocket, with the adjacent uranyl-oxo unit representing the most likely HAA site.

Investigation of the double HAA by deuterium labelling

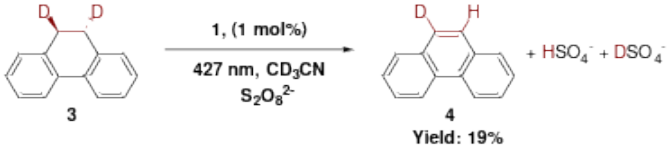

Scheme 2 Dehydrogenation of trans-d_2-dihydrophenanthrene ($C_{14}H_{10}D_2$, **3**) furnishing phenanthrene-9-d_1 ($C_{14}H_9D$, **4**) catalyzed by **1**.

The addition of a base (2,6-lutidine) does not improve the cyclooctene yield (**Fig. S52** and **S53**), arguing against a yield-limiting protonated oxo (either uranyl or POM – centered) intermediate.

We synthesized trans-d_2-dihydrophenanthrene ((9S,10S)-9,10-dihydrophenanthrene-9,10-d_2, $C_{14}H_{10}D_2$, **3**) (**Fig. S54–S57**) as a fused substrate to investigate the nature of the dehydrogenation mechanism. Formation of exclusively monodeuterated phenanthrene ($C_{14}H_9D$, **4**) as the dehydrogenation product (**Scheme 2, S5**) is consistent with a stereospecific, *syn*-type abstraction of adjacent C–H/D bonds at the 9,10 positions and supports a cooperative pathway within the pre-organized di-uranyl/POM pocket (**Scheme 2, Fig. 3, S58** and **S59**). The exclusive formation of the d_1 product also indicates that the reaction is not being governed by a strong intramolecular primary kinetic isotope effect,[54] which would selectively favor C–H over C–D cleavage (**Fig. 3, S58** and **S59**).

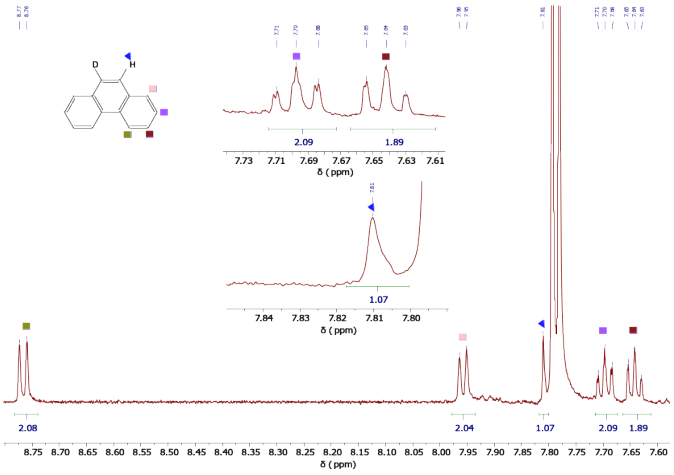

Figure 3 ^1H NMR spectrum of a CD_3CN solution containing **1** (1 eq., 1 mol%) with 100 equiv. $TBA_2S_2O_8$ and 100 equiv. (9S,10S)-9,10-dihydrophenanthrene-9,10-d_2 ($C_{14}H_{10}\mathbf{D_2}$) following 16 hours of irradiation at 52 W, 427 nm. The reaction was carried out in dry CD_3CN to minimize interference from adventitious proton sources that could otherwise bias the observed isotopomer distribution.^1H NMR (600 MHz, CD_3CN) δ 8.77 (d, J = 8.3 Hz, 2H), 7.96 (d, J = 7.9 Hz, 2H), 7.81 (s, 1H), 7.70 (t, J = 7.6 Hz, 2H), 7.64 (t, J = 7.3 Hz, 2H).

This *syn*-configuration of the two HAA steps, combined with the other observations, leads us to propose the photocatalytic dehydrogenation reaction in Scheme 3.

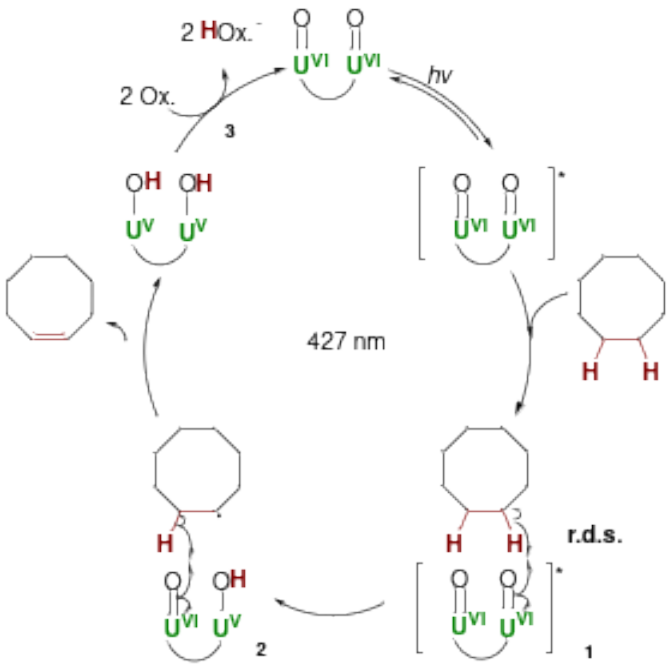

Scheme 3 Proposed mechanism of photocatalytic dehydrogenation of cyclooctane. The depicted U(V)–OH/U(V)–OH species is intended as a simplified representation of the reduced, protonated uranyl-oxo sites following HAA, rather than as the assignment of a long-lived resting state.

This starts with the photo-excitation of **1** to an excited state in which one oxo group behaves as an oxo-centered U^{V}–$O^{\cdot}$ radical and abstracts a $H^{\cdot}$ via d-HAT from the cyclooctane substrate (Scheme 3, step 1) furnishing a cyclooctyl radical. Consecutive thermal HAA on the weakened vicinal C–H[55] bond (Scheme 3, step 2) forms the cyclooctene product. While this step is consistent with cooperative involvement of the paired uranyl sites, participation of a nearby POM oxo site in a coupled H-transfer/proton-transfer event cannot be excluded. The catalytic cycle is closed by oxidative regeneration of **1** by $S_2O_8^{2-}$ or chloranil ($C_6Cl_4O_2$) forming HSO_4^- or 2,3,5,6-tetrachlorobenzene-1,4-diol ($C_6Cl_4(OH)_2$) respectively (Scheme 3, step 3).

Conclusions

In summary, the lacunary germanotungstate [γ-$Ge^{IV}W_{10}O_{34}(H_2O)_2]^{4-}$ forms a rigid scaffold that enforces close proximity between two accessible $\{UO_2\}^{2+}$ centers in the new $[NBu^n_4]_8[(UO_2)_2(GeW_{10}O_{34}(\mu_2\text{-}OH)_2)_2]$ **1**. Soluble in organic solvents, **1** mediates visible-light-driven photocatalytic dehydrogenation of inert alkanes such as cyclooctane, a reaction not observed in mononuclear uranyl analogues. Catalytic yields of up to 73% are measured for 9,10-dihydrophenanthrene to phenanthrene (TON per molecule = 73). Mechanistic data support a HAA-initiated radical pathway in which the first C–H cleavage is turnover-limiting (primary KIE $k_H/k_D = 3.16$), while $S_2O_8^{2-}$ serves as an external oxidant and does not enter the rate law. Radical-trapping experiments and Stern–Volmer studies are consistent with carbon-radical intermediates, and stereochemical/isotope probes point to cooperative, *syn*-hydrogen atom abstractions.

Taken together, these results establish a concrete design principle for actinide photocatalysis: supporting two uranyl cations within an oxidatively robust framework can unlock cooperative bond-activation chemistry inaccessible to mononuclear analogues. Future work will focus on tuning excited-state properties to broaden substrate scope and improve selectivity, positioning di-uranyl platforms as mild alternatives to precious-metal dehydrogenation catalysts.

Experimental

Synthesis of $[NBu^n_4]_8[(UO_2)_2\{GeW_{10}O_{34}(\mu_2\text{-}OH)_2\}_2]\cdot(CH_3)_2CO$ (1)

To a stirred colorless solution of $[(n\text{-}C_4H_9)_4N]_4[\gamma\text{-}GeW_{10}O_{34}(H_2O)_2]$ (H_2**GeW$_{10}$**) (250 mg, 0.072 mmol) in acetone/water (5 mL/80 µL) $[UO_2(acac)_2(H_2O)_2]$ (33.8 mg, 0.072 mmol, 1 equiv. with respect to (H_2**GeW$_{10}$**)) was added and the resulting yellow solution was stirred for 90 min at RT (about 20 °C). The yellow solution was layered with diethyl ether (1.25 mL) resulting in diffraction-quality yellow block shaped crystals of $[NBu^n_4]_8[(UO_2)_2(GeW_{10}O_{34}(\mu_2\text{-}OH)_2)_2]\cdot(CH_3)_2CO$ (**1**) being deposited overnight. Yield: 120 mg, 25 % based on U. Elemental analysis calcd. (found) for $C_{131}H_{298}N_8O_{77}U_2Ge_2W_{20}$ ($(C_{16}H_{36}N)_8[(UO_2)_2(GeW_{10}O_{34}(\mu_2\text{-}OH)_2)_2]\cdot(CH_3)_2CO$): C 20.93 (20.84), H 4.00 (3.92), N 1.49 (1.45).

General procedure for photocatalytic studies

A 3 mL ampoule equipped with a stir bar was charged with a solution of the hydrocarbon substrate (6×10^{-5} mol, 0.06 M) and $\{UO_2\}^{2+}$ photocatalyst (6×10^{-7} mol, 1 mol%) in acetonitrile (1 mL). An aqueous solution of $Na_2S_2O_8$, (14 mg, 6×10^{-5} mol in 200 µL H_2O) was then added. The mixture was degassed by three freeze–pump–thaw cycles and placed under an argon atmosphere. The sealed ampoule was magnetically stirred (~100 rpm) at a distance of 5 cm from two 427 nm LED lamps (Kessil PR160L 427, positioned on opposite sides). The reaction temperature was continuously monitored and maintained at 28–30 °C using a fan for cooling. Following 24h of irradiation, 500 µL of the reaction mixture was transferred to a coaxial NMR tube containing an internal standard (methyl acetate, 20 µL in 500 µL acetonitrile). The yield of the dehydrogenated product was calculated by comparing the integral of the multiplet assigned to the olefinic C–H (2H) to the methyl acetate peak (3.67–3.45 ppm, m, 3H).

General procedure for photocatalytic studies under anaerobic conditions

In a N_2 filled glovebox, a 3 mL ampoule equipped with a stir bar was charged with $Na_2S_2O_8$ (14 mg, 6×10^{-5} mol). To the solid $Na_2S_2O_8$, a solution of the hydrocarbon substrate (6×10^{-5} mol, 0.06 M) and photocatalyst **1** (6×10^{-7} mol, 1 mol%) in acetonitrile (1.2 mL) was then added, affording a white suspension. The

sealed ampoule was removed from the glovebox and magnetically stirred (~1000 rpm) at a distance of 5 cm from two 427 nm LED lamps (Kessil PR160L 427, positioned on opposite sides). The reaction temperature was maintained at 29(±1) °C. Following 24h of irradiation, 500 µL of the reaction mixture was analyzed by NMR spectroscopy in a coaxial NMR tube containing an internal standard (methyl acetate, 20 µL in 500 µL acetonitrile). The yield of the dehydrogenated product was calculated by comparing the integral of the multiplet assigned to the olefinic C–H (2H) to the methyl acetate resonance (3.67–3.45 ppm, m, 3H).

Author contributions

ET, GH and CSC: experiments. ET and PLA: project conceptualization, funding acquisition. PLA: funding acquisition, supervision. All authors: analysis, writing & editing.

Conflicts of interest

There are no conflicts to declare.

Data availability

Crystallographic data are deposited at CCDC, code 2530061 and can be obtained from https:// www.ccdc.cam.ac.uk. Open data are available at 10.17632/trktrdxywh.1

The data supporting this article have been included as part of the supplementary information (SI). Supplementary information: synthetic and mechanistic details. See DOI: https://doi.org/10.1039/d6sc01626j.

Acknowledgements

We thank the Catalysis Program (catalysis studies), FWP CH030201, and the Rare Earth Project in the Separations Program (photoluminescence spectroscopy), FWP CH20CRIMAT of the U.S. Department of Energy (DOE), Office of Science, Office of Basic Energy Sciences, Chemical Sciences, Geosciences, and Biosciences Division at the Lawrence Berkeley National Laboratory under Contract DE-AC02- 05CH11231 for the support of this work. E.T. thanks the Austrian Science Fund (FWF) for an Erwin Schrödinger Fellowship (Grant-DOI 10.55776/J4851). C.S.C. was supported under a Department of Energy Nuclear Energy University Programs Graduate Fellowship DE-NE0009073. We thank Drs Hasan Celik, Raynald Giovine, and Pines Magnetic Resonance Center's Core NMR Facility (PMRC Core) for spectroscopic assistance. The instrument used in this work was in part supported by NIH S10OD024998. We are grateful to Prof. Robert G. Bergman for helpful discussions.

Notes and references

1. K. I. Goldberg and A. S. Goldman, *Accounts of Chemical Research*, 2017, **50**, 620-626.
2. R. H. Crabtree, M. F. Mellea, J. M. Mihelcic and J. M. Quirk, *Journal of the American Chemical Society*, 1982, **104**, 107-113.
3. R. H. Crabtree, J. M. Mihelcic and J. M. Quirk, *Journal of the American Chemical Society*, 1979, **101**, 7738-7740.
4. D. Baudry, M. Ephritikhine and H. Felkin, *Journal of the Chemical Society, Chemical Communications*, 1980, 1243–1244.
5. X. Zhang, S.-B. Wu, X. Leng, L. W. Chung, G. Liu and Z. Huang, *ACS Catalysis*, 2020, **10**, 6475-6487.
6. B. M. Gordon, N. Lease, T. J. Emge, F. Hasanayn and A. S. Goldman, *Journal of the American Chemical Society*, 2022, **144**, 4133-4146.
7. P. P. Singh, S. Sinha, P. Gahtori, S. Tivari and V. Srivastava, *Organic & Biomolecular Chemistry*, 2024, **22**, 2523-2538.
8. M. T. Pope, Y. Jeannin and M. Fournier, *Heteropoly and isopoly oxometalates*, Springer, 1983.
9. M. Bösing, A. Nöh, I. Loose and B. Krebs, *Journal of the American Chemical Society*, 1998, **120**, 7252-7259.
10. S.-S. Wang and G.-Y. Yang, *Chemical Reviews*, 2015, **115**, 4893-4962.
11. M. Sadakane and E. Steckhan, *Chemical Reviews*, 1998, **98**, 219-238.
12. J. M. Clemente-Juan, E. Coronado and A. Gaita-Ariño, *Chemical Society Reviews*, 2012, **41**, 7464-7478.
13. A. Bijelic, M. Aureliano and A. Rompel, *Chemical Communications*, 2018, **54**, 1153-1169.
14. A. Bijelic, M. Aureliano and A. Rompel, *Angewandte Chemie International Edition*, 2019, **58**, 2980-2999.
15. H.-J. Zhai, B. Kiran, L.-F. Cui, X. Li, D. A. Dixon and L.-S. Wang, *Journal of the American Chemical Society*, 2004, **126**, 16134-16141.
16. M. S. Chen and M. C. White, *Science*, 2010, **327**, 566-571.
17. T. Nanjo, E. C. de Lucca, Jr. and M. C. White, *Journal of the American Chemical Society*, 2017, **139**, 14586-14591.
18. O. Y. Lyakin, E. P. Talsi and K. P. Bryliakov, *ACS Catalysis*, 2025, **15**, 17525-17547.
19. M. D. Tzirakis, I. N. Lykakis and M. Orfanopoulos, *Chemical Society Reviews*, 2009, **38**, 2609-2621.
20. J. G. West, D. Huang and E. J. Sorensen, *Nature Communications*, 2015, **6**, 10093.
21. M.-J. Zhou, L. Zhang, G. Liu, C. Xu and Z. Huang, *Journal of the American Chemical Society*, 2021, **143**, 16470-16485.
22. R. A. Jagtap, Y. Nishioka, S. M. Geddis, Y. Irie, T. Takanashi, R. Adachi, A. Yamakata, M. Fuki, Y. Kobori, H. Mitsunuma and M. Kanai, *Nature Communications*, 2025, **16**, 428.
23. B. E. Cowie, J. M. Purkis, J. Austin, J. B. Love and P. L. Arnold, *Chemical Reviews*, 2019, **119**, 10595-10637.
24. D. Hu and X. Jiang, *Synlett*, 2021, **32**, 1330-1342.
25. W.-D. Wang, A. Bakac and J. H. Espenson, *Inorganic Chemistry*, 1995, **34**, 6034-6039.
26. Y. Mao and A. Bakac, *Inorganic Chemistry*, 1996, **35**, 3925-3930.
27. J. G. West, T. A. Bedell and E. J. Sorensen, *Angewandte Chemie International Edition*, 2016, **55**, 8923-8927.
28. P. L. Arnold, J. M. Purkis, R. Rutkauskaite, D. Kovacs, J. B. Love and J. Austin, *ChemCatChem*, 2019, **11**, 16, 3786–3790.
29. R. Rutkauskaite, X. Zhang, A. W. Woodward, Y. Liu, G. Herrera, J. Purkis, S. D. Woodall, M. Sarsfield, G. Schreckenbach, L. S. Natrajan and P. L. Arnold, *Chemical Science*, 2024, **15**, 6965-6978.

30. L. Capaldo, D. Merli, M. Fagnoni and D. Ravelli, *ACS Catalysis*, 2019, **9**, 3054-3058.
31. G. Herrera, A. Wong, D. Fiszbein, B. A. Haibel, J. Lara, N. J. Katzer, J. F. Hartwig and P. L. Arnold, *J. Am. Chem. Soc.* 2026, **148**, 21933-21942.
32. Y. Liu, R. Rutkauskaite, F. Y. T. Lam, A. R. Wong and P. L. Arnold, presented in part at the ACS Fall 2023, San Francisco, CA, USA, 2023. DOI. https://data.mendeley.com/preview/cx5hm4fh5k?a=73faf77a-5343-415c-a28a-1e1c7f8b27b8
33. X. Ma, H. Li, L. Chen and J. Zhao, *Dalton Transactions*, 2016, **45**, 4935-4960.
34. G.-P. Yang, X.-L. Zhang, Y.-F. Liu, D.-D. Zhang, K. Li and C.-W. Hu, *Inorganic Chemistry Frontiers*, 2021, **8**, 4650-4656.
35. J.-H. Ding, Y.-F. Liu, Z.-T. Tian, P.-J. Lin, F. Yang, K. Li, G.-P. Yang and Y.-G. Wei, *Inorganic Chemistry Frontiers*, 2023, **10**, 3195-3201.
36. X. Wang, M. Cheng, Y. Liu, D. Zhang and J. Niu, *Inorganic Chemistry*, 2025, **64**, 11561-11570.
37. K. Sugahara, T. Kimura, K. Kamata, K. Yamaguchi and N. Mizuno, *Chemical Communications*, 2012, **48**, 8422-8424.
38. K. Kamata, K. Sugahara, K. Yonehara, R. Ishimoto and N. Mizuno, *Chemistry – A European Journal*, 2011, **17**, 7549-7559.
39. K. Kamata, K. Yonehara, Y. Sumida, K. Yamaguchi, S. Hikichi and N. Mizuno, *Science*, 2003, **300**, 964-966.
40. E. Tanuhadi, E. Al-Sayed, A. Roller, H. Čipčić-Paljetak, D. Verbanac and A. Rompel, *Inorganic Chemistry*, 2020, **59**, 14078-14084.
41. B. S. Bassil and U. Kortz, *Dalton Transactions*, 2011, **40**, 9649-9661.
42. E. J. Baran and B. S. Parajón Costa, *An. Asoc. Quim. Argent.*, 2021, **108**, 1–9.
43. A. J. Gaunt, I. May, R. Copping, A. I. Bhatt, D. Collison, O. Danny Fox, K. Travis Holman and M. T. Pope, *Dalton Trans.*, 2003, 3009-3014.
44. T. J. Johnson, L. E. Sweet, D. E. Meier, E. J. Mausolf, E. Kim, P. F. Weck, E. C. Buck and B. K. McNamara, *The Journal of Physical Chemistry A*, 2015, **119**, 9996-10006.
45. M. Autillo, R. E. Wilson, M. Vasiliu, G. F. de Melo and D. A. Dixon, *Inorganic Chemistry*, 2022, **61**, 15607-15618.
46. L.-H. Bi, B. Li, L.-X. Wu and Y.-Y. Bao, *Inorganica Chimica Acta*, 2009, **362**, 3309-3313.
47. H. D. Burrows and T. J. Kemp, *Chemical Society Reviews*, 1974, **3**, 139-165.
48. E. Al-Sayed, S. P. Nandan, E. Tanuhadi, G. Giester, M. Arrigoni, G. K. H. Madsen, A. Cherevan, D. Eder and A. Rompel, *ChemSusChem*, 2021, **14**, 2529-2536.
49. M. Galeotti, M. Salamone and M. Bietti, *Chemical Society Reviews*, 2022, **51**, 2171-2223.
50. S. Cao and L. Piao, *Angewandte Chemie International Edition*, 2020, **59**, 18312-18320.
51. A. E. Shilov and G. B. Shul'pin, *Chemical Reviews*, 1997, **97**, 2879-2932.
52. Z. Lu, M. Dagar, J. R. McKone and E. M. Matson, *Chemical Science*, 2025, **16**, 6736-6743.
53. Z. Lu, S. E. Cooney, J. R. McKone and E. M. Matson, *JACS Au*, 2024, **4**, 1310-1314.
54. E. M. Simmons and J. F. Hartwig, *Angewandte Chemie International Edition*, 2012, **51**, 3066-3072.
55. X.-M. Zhang, *The Journal of Organic Chemistry*, 1998, **63**, 1872-1877.